

Mott insulating negative thermal expansion perovskite TiF_3

Donal Sheets, Kaitlin Lyszak, Menka Jain, Gayanath W.

Fernando, Ilya Sochnikov, Jacob Franklin, and Jason N. Hancock

*Department of Physics, University of Connecticut, Storrs, Connecticut, 06269 USA and
Institute for Materials Science, University of Connecticut, Storrs, Connecticut, 06269 USA*

R. Matthias Geilhufe

Department of Physics, Chalmers University of Technology, 412 96 Göteborg, Sweden

(Dated: November 15, 2023)

We characterize perovskite TiF_3 , a material which displays significant negative thermal expansion at elevated temperatures above its cubic-to-rhombohedral structural phase transition at 330 K. We find the optical response favors an insulating state in both structural phases, which we show can be produced in density functional theory calculations only through the introduction of an on-site Coulomb repulsion. Analysis of the magnetic susceptibility data gives a $S=\frac{1}{2}$ local moment per Ti^{+3} ion and an antiferromagnetic exchange coupling. Together, these results show that TiF_3 is a strongly correlated electron system, a fact which constrains possible mechanisms of strong negative thermal expansion in the $\text{Sc}_{1-x}\text{Ti}_x\text{F}_3$ system. We consider the relative strength of the Jahn-Teller and electric dipole interactions in driving the structural transition.

I. INTRODUCTION

Materials based on the perovskite lattice structure have garnered sustained interest for over a century, largely because its accommodation of ionic substitutions permits a wide range of effective controls with which one can explore quantum matter. Along with its natural cascade of structural phases, the perovskite lattice produces opportunities to promote phase competition and pursue exotic behavior as demonstrated with the discovery of colossal magnetoresistance[1], high- κ dielectricity[2], strong negative thermal expansion (NTE)[3, 4], and high-temperature superconductivity[5]. Within the context of these discoveries, technological advances such as ion-shuttling[6] and solar harvesting[7] relevant to energy applications have been demonstrated. The transition metal fluoride perovskites are much less studied than their oxide cousins, and display marked differences. At the level of considering whether chemically stable systems could exist, oxide perovskites have a typical form ABO_3 , where the nominal valence sum of the A and B sites is near +6. There are very few examples of A-site free oxide perovskites, ReO_3 and MoO_3 among them[3], consistent with the rarity of hexavalent single ions. The fluoride perovskites however, with typical formula unit BF_3 , require only a trivalent B site, which is common across the d -filling transition metal series ($\text{B}=\text{Sc}, \text{Ti}, \text{V}, \text{Cr}, \text{Mn}, \text{Fe}, \text{Co}, \text{Ni}$)[4, 8–11].

Among the many potential BF_3 materials based on $3d$ -filling transition metal B ions, the end member ScF_3 is particularly simple electronically and magnetically. Considering Pauling valence counting returns a d^0 configuration for this ion, which is fully consistent with the large electronic band gap both observed via resonant photoemission[16] and computed using density functional theory methods[17] as well as its diamagnetic response[18]. There is however a rich and robust phys-

ical peculiarity in this system, in particular the sizable *negative* thermal expansion coefficient ($\alpha_L \geq -14$ ppm/K) present over a 1000 K temperature window[4]. Soft mode spectroscopy using inelastic X-ray scattering has determined that the ground state of this system resides very close to a structural quantum phase transition between the cubic highly symmetric $Pm\bar{3}m$ and a lowered-symmetry cell-doubled rhombohedral $R\bar{3}c$ structure[13]. It is widely believed that the associated strong transverse fluctuations of the F ions are responsible for the NTE in ScF_3 [19–21], although the degree of atomic correlation within the unit cell is debated[22, 23]. Research into the anomalous NTE of trifluorides is a very active area[4, 12, 13, 15, 17–32], since ScF_3 displays behavior typical of a broader class of more complex systems such as ZrW_2O_8 and related materials which also show very soft phonon modes and display strong negative thermal expansion[33–35].

Perturbations of the structural quantum phase transition and strong NTE behavior using ionic substitution on the trivalent Sc^{+3} site in $\text{Sc}_{1-x}\text{X}_x\text{F}_3$ has revealed the NTE behavior to be persistent at elevated temperatures for $\text{X}=\text{Al}, \text{Y}, \text{Ti}, \text{Ga}, \text{Fe}$ over a significant span of compositions[12, 18, 24, 25]. The opportunity to compositionally introduce electronic degrees of freedom in a system with a structurally critical ground state is an exciting prospect, particularly in light of the high interest in low-carrier superconductivity in elemental bismuth[36] as well as incipient-ferroelectric perovskites SrTiO_3 [37] and KTaO_3 [38]. The substitution $\text{X}=\text{Ti}$ in particular permits ionic substitution over its entire compositional range[25] and appears to accordingly introduce muted disorder effects[28] in comparison to other substitutions ($\text{X}=\text{Al}, \text{Y}$). Figure 1a summarizes the known phase diagram of $\text{Sc}_{1-x}\text{Ti}_x\text{F}_3$, showing a structurally lowered $R\bar{3}c$ symmetry for all temperatures below its structural transition temperature $T_s(x) \simeq 340\text{K} \times x$. This phase boundary along with the documented pressure behavior has

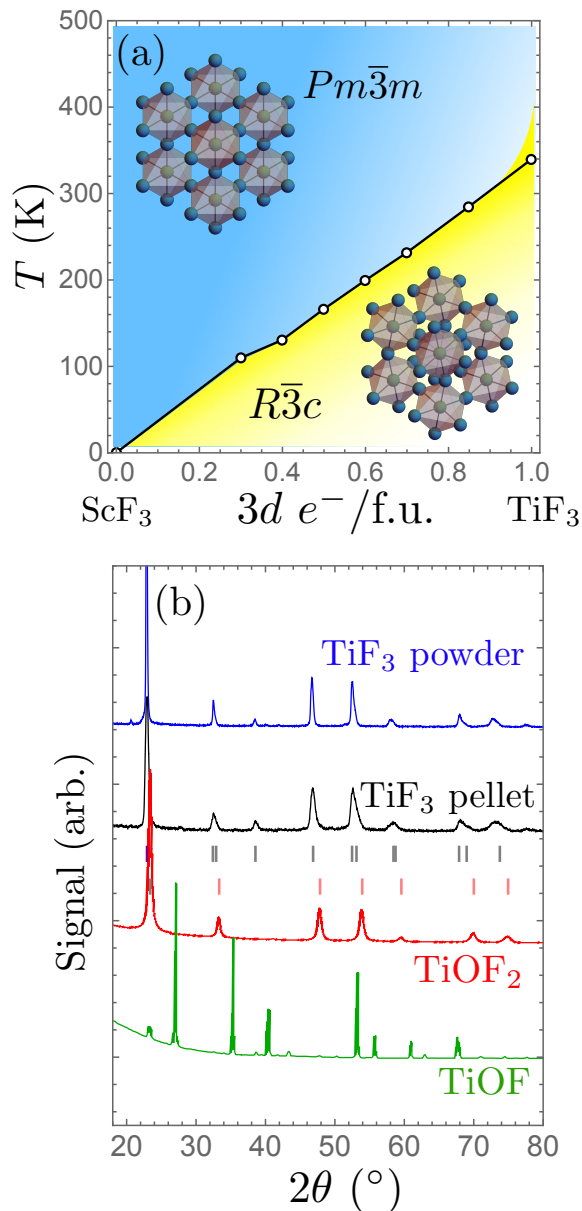


FIG. 1. (a) Structural phase diagram of $\text{Sc}_{1-x}\text{Ti}_x\text{F}_3$. The horizontal axis is the x in this composition, which also corresponds to the expected $3d$ filling in this system. Structural data are from refs. [12] and [13]. (b) X-ray diffraction data on loose TiF_3 powder (blue), pelletized TiF_3 powder (black), and for comparison X-ray diffraction data on possible oxidation products TiOF_2 ($Pm\bar{3}m$ structure, ref. [14]) and TiOF ($P4_2/mnm$, ref. [15]). No peaks from either oxide are present in the samples presented here. Vertical bars show the expected diffraction peaks for TiF_3 (black) and TiOF_2 (red).

been analyzed using a Landau-Ginzberg-Devonshire approach to identify some compositions in this series with strong promise for enabling near-ambient barocaloric refrigeration[29]. Of basic interest is whether doping ScF_3 with electrons to produce TiF_3 results in a metallic or insulating state, and whether there is any long range

magnetic order resultant from spin exchange interactions. At least two distinct possibilities have been presented in a prior theoretical work[39]: a ferromagnetic half metal in the uncorrelated ($U = 0$) limit where the calculations are well controlled, versus incorporating electronic correlation ($U \simeq 8$ eV) predicts an antiferromagnetic insulator with spin- $\frac{1}{2}$ moments. In this work, we constrain the electronic and magnetic status of TiF_3 in a combined study of its structural, magnetic, and electronic properties[39].

II. STRUCTURAL CHARACTERIZATION

Powder samples of TiF_3 sourced from Sigma-Aldrich were used in this study and phase purity was confirmed using X-ray diffraction. Figure 1b shows room temperature powder diffraction scans from a pressed pellet and loose powder collected from a Bruker D2 Phaser diffractometer and a Cu X-ray source. Also shown are the expected Bragg peak positions for potential oxide impurities TiOF [15] and TiOF_2 [14]. All observed peaks can be assigned to the expected $R\bar{3}c$ Bragg reflections of TiF_3 , confirming phase purity of both powder and pressed pellet samples used in this study. As expected, the pressed pellet shows significantly broader Bragg peaks, likely a result of the complex strain texture in these samples which gives a broader distribution of lattice parameters compared to the loose powder samples. A refinement of the powder data produces the $R\bar{3}c$ space group structure with rhombohedral lattice parameters consistent with prior work[8, 12].

III. INFRARED REFLECTIVITY

To assess the electronic status of TiF_3 , we seek information on the transport characteristics, which can be challenging in granular samples. Another option besides direct transport measurements is to extrapolate the far-infrared optical response to the static limit, where metals and insulators have strongly contrasting frequency-dependent behavior. Far-infrared reflectivity $R(\omega)$ measurements were conducted using a hydraulically-pressed pellet which was half-coated with gold using a thermal evaporator source. A spectrum taken from the optically thick gold film provides an appropriate reference spectrum which is divided by the sample spectrum to determine the reflectivity. The data were collected using a Bruker 66v Fourier transform infrared spectrometer (FTIR) with a customized chamber suited for near-normal incidence reflectivity. The spectra were collected using a helium-cooled bolometer covering the spectral range $80\text{--}1000$ cm^{-1} using a layered mylar beam splitter and a silicon carbide globar as a radiation source. To enable these measurements at high temperatures, crossing the cubic-to-tetragonal structural phase transition at $T_s=340$ K and beyond to the high temperatures $T > 420$ K where NTE has been reported, we built a

special high-temperature infrared reflectivity apparatus and affixed our sample to a silicon carbide heater element using a high temperature ceramic paste. A dc controllable power supply was used to drive the heater element and a K-type thermocouple monitored the local sample temperature during the measurement.

Figure 2 shows the temperature-dependent reflectivity of a pelletized TiF_3 sample. In all measured spectra, two strong and broad reststrahlen bands are apparent, very similar to those seen in the single crystal ScF_3 reflectivity[27], plotted for comparison. We see these features persist when the sample is heated above the structural phase transition and to elevated temperatures where NTE was reported[25]. Similar infrared response has been observed in both powdered[31] and single-crystal ScF_3 and attributed to the presence of two infrared-active transverse optical phonons[19]. The relative broadening of the reststrahlen bands in the pelletized sample is likely a result of inhomogeneous broadening due to a complex stress state of the packed powder sample, an effect which is potentially exacerbated by the known pressure-tuned ferroelastic structural transition near room temperature[8, 12].

Importantly, the reflectivity in the dc limit tends toward a constant around $R(\omega \rightarrow 0) \simeq 0.3$ for all temperatures, which is strong evidence that TiF_3 is an insulator. If any free carriers are present in the system, no static field could exist in the material bulk, and one consequently expects $R(\omega \rightarrow 0) \rightarrow 1$, which is clearly not the case. This optical determination of insulating behavior is fully consistent with our attempts to measure resistance using a multimeter probe on the same pressed pellet. The low-frequency dielectric constant may also be estimated from the low-frequency reflectance value of $\simeq 0.3$ using Fresnel's equations. We find, using $R(\omega \rightarrow 0) = |(\sqrt{\epsilon_0} - 1)/(\sqrt{\epsilon_0} + 1)|^2$ that the static dielectric function of TiF_3 is $\epsilon_0 \simeq 11.7$, similar to that of pure silicon, and significantly higher than for ScF_3 , where $\epsilon_0 \simeq 5.8$. Since the phonon spectral weight is expected to be very similar, the enhanced polarizability of TiF_3 must be attributable to interband transitions at higher frequency, consistent with the Lydan-Sachs-Teller relation[40, 41]. Indeed, TiF_3 has a gray appearance, while ScF_3 is transparent, suggesting a much lower energy electronic threshold in TiF_3 . We conclude that TiF_3 is an insulator in both structural phases of interest and return to the electronic structure below in section V.

IV. MAGNETIC SUSCEPTIBILITY

Having established that TiF_3 shows the infrared response expected of an insulator, we probed its magnetic response to determine whether this is a correlated or band-type insulating system. Magnetic susceptibility measurements were performed in a Quantum Design Physical Property Measurement System. Loose powder was sealed in a nylon capsule in a helium-purged en-

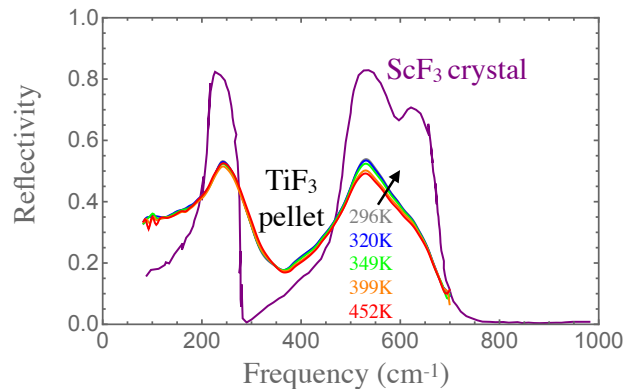


FIG. 2. Optical reflectivity of packed powder TiF_3 at different temperatures crossing from the rhombohedral to cubic structures, where negative thermal expansion has been reported. For comparison, reflectivity of single crystal ScF_3 (purple) is shown. Both samples were half coated with a gold film as a reference. Two broad reststrahlen bands show that both systems are insulating.

vironment for improved thermalization and to mitigate potential oxidation during thermal cycling and material handling. A static field H was applied with a small probing ac field varying at frequency f . The in-phase (M') and out-of-phase (M'') components of the magnetization were measured and the in-phase ($\chi' = M'/H$) and out-of-phase ($\chi'' = M''/H$) AC susceptibility was computed. Figure 3a shows AC magnetic susceptibility χ' with an applied field of 100 Oe varying at frequencies between 1-5 kHz. The Curie-like response appears identical at all measured frequencies, consistent with the presence of local moments in TiF_3 . The Figure 3a inset shows a plot of $1/\chi'$ for the lowest frequency only along with a fit of data above 20 K to the Curie-Weiss form. Using the high-temperature data $T > 30$ K, and performing a least-squares fit to the conventional Curie-Weiss law $\chi(T) = C/(T - \theta_W)$ (dotted line) the Weiss temperature is found to be $\theta_W \simeq -13.8$ K with a Curie constant $C = 0.247$ emu/K. The Curie constant gives an effective magnetic moment of $\mu_{eff} = 1.40 \mu_B$ per Ti. This value is roughly eighty percent the expected value of $1.73 \mu_B$ for one spin-1/2 localized electron per Ti^{+3} ion. This local magnetic moment is significantly larger than that of single crystal TiOF which was recently found to be $\mu_{eff} = 0.95 \mu_B$ per Ti and a similar Weiss temperature $\theta_W \simeq -19.3$ K [15]. In that system, a Pauli paramagnetic component was needed to fit the data there and it was suggested that TiOF is partially metallic, or at least near the threshold of electronic delocalization, potentially explaining the significantly lower moment than in TiF_3 .

Figure 3b shows the out of phase susceptibility χ'' , which is consistent with zero for all temperatures above 10 K but shows a steep rise at lower temperature, about 1% of the in phase part in total. Figure 3c shows the quantity $\frac{d}{dT}(\frac{1}{\chi'})$, which shows clear change of behavior below 10 K. Together, these data suggest a magnetic

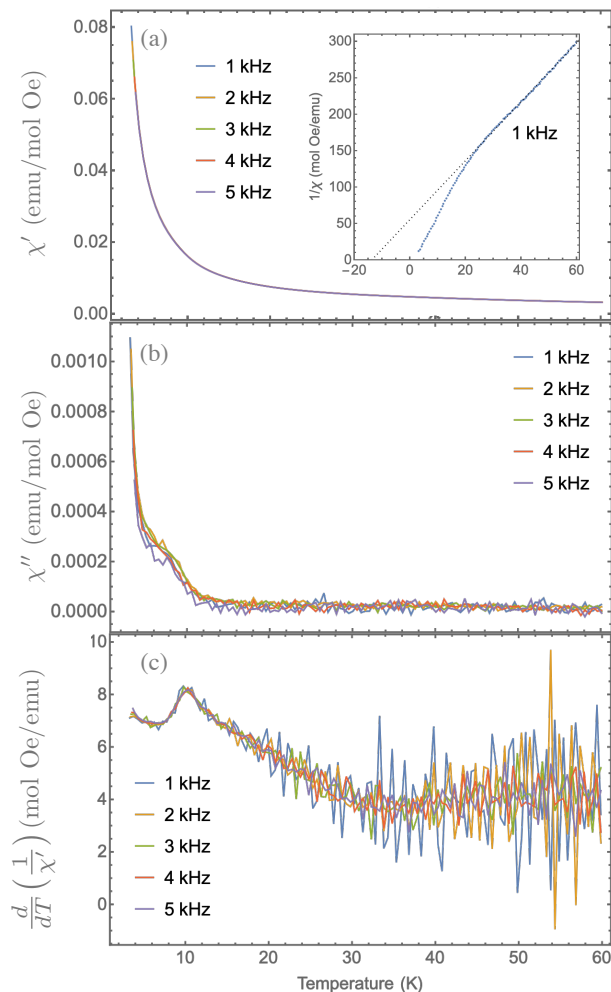


FIG. 3. (a) The in-phase part of the AC susceptibility χ' taken at 100 Oe from TiF_3 at five low frequencies. The inset shows the data for 1kHz plotted as $1/\chi'$ to demonstrate the quality of fit and determination of the antiferromagnetic Weiss temperature $\theta_W = -13.8\text{K}$. (b) The out-of-phase AC susceptibility χ'' shows weak features below 10 K. (c) Temperature derivative of the in-phase susceptibility $\frac{d}{dT} \left(\frac{1}{\chi'} \right)$, exposing the features of a magnetic transition below 10K.

transition below 10 K. Future neutron magnetic diffraction or resonant X-ray scattering could be used to identify the magnetic state. It is noteworthy that a prior neutron scattering study found an absence of magnetic order down to 10 K[39], consistent with the results shown here.

V. ELECTRONIC STRUCTURE CALCULATIONS

We have shown that the optical response of TiF_3 is consistent with a correlated insulating state with local moment magnetism. To contextualize these results, we have performed first-principles calculations, both on a

full rhombohedral unit cell (space group $R\bar{3}c$, #167) as well as on a symmetry-reduced triclinic cell. In comparison to other work[39], we have used a larger unit cell containing 6 Ti and 18 F atoms and also permitted the possibility of non-collinear magnetism. These calculations were carried out within the framework of the density functional theory[42, 43], as implemented in the Vienna Ab Initio Simulation Package (VASP) [44]. The exchange-correlation functional was approximated by the generalized gradient approximation (GGA) [45], with the energy cutoff chosen according to potential input files. For integration in \vec{k} -space, a $6 \times 6 \times 6$ (triclinic cell) Γ centered mesh according to Monkhorst and Pack [46] was used during each self-consistent cycle. Several smaller-cell calculations were also run with a $10 \times 10 \times 4$ Γ -centered mesh. Structural optimization was performed until the Hellman-Feynman forces acting on the atoms were negligible.

Figure 4 shows the density of states calculated for different values of the electronic correlation parameter U in the large cell (Ti_6F_{18}) calculations, which permit freedom for structural optimization compared to prior work. The behavior of the d -electrons becomes quite evident from the density of states. In the insulating ($U \geq 3$ eV) cases shown, there is a well separated density of states peak just below the gap. A count of the total number of electrons in this sharp feature of the density of states yields nearly exactly one d electron per Ti atom, consistent with the measured long moment. Consistent with prior work[32, 39], in the uncorrelated $U=0$ eV limit, the calculation produces a finite density of states at the chemical potential $E=0$ for the majority spin species while the electronic states with minority spin are conversely gapped. This structure describes a fully spin polarized ferromagnetic half metal, which is clearly inconsistent with the experimental evidence presented here. In contrast, invocation of even a moderate correlation parameter $U=3$ eV [47–49] predicts the development of a gap spanning the chemical potential and an insulating state in the correlated limit. Increasing this parameter to $U=6$ eV further widens this gap, consistent with prior work[39]. We conclude that correlated electron physics are required in a minimal set of considerations to describe the observed behavior presented here. Interestingly, the degree of correlation required to separate the antiferromagnetic insulating and fully spin-polarized itinerant ferromagnetic half-metal state is rather small. While most calculations are limited exactly at the boundary between these two states[50], these considerations bolster our assignment of TiF_3 as residing at the Mott insulator side of this putative transition and demonstrate the failure of uncorrelated approaches in describing the electronic and magnetic ground state.

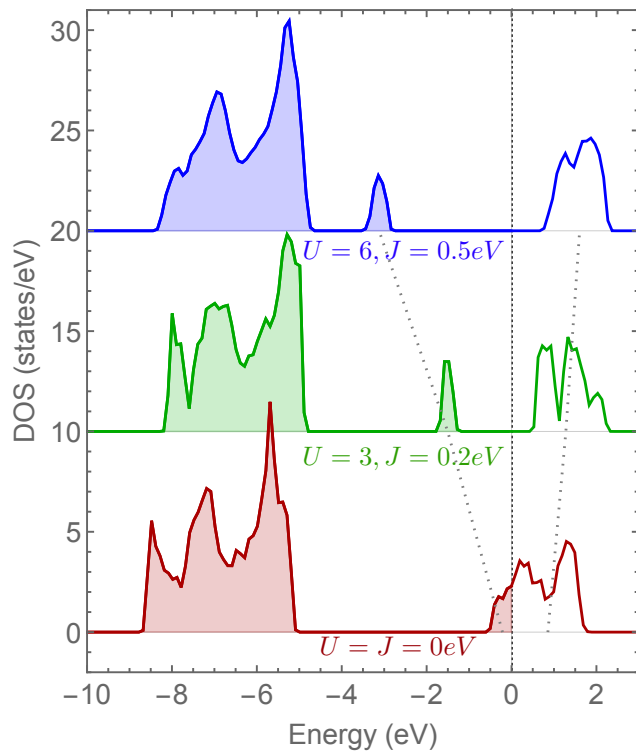


FIG. 4. Electronic structure calculations showing the evolution of TiF_3 responsive to different values of the correlation parameter U and computed in the GGA+ U scheme. The dashed lines track the computed centroid of the unoccupied and occupied d states and are a guide to the eye. $U=0$ corresponds to a ferromagnetic half metal while even modest U values open a sizable correlation gap and favor magnetic order of localized moments.

VI. DISCUSSION

The realization that TiF_3 is a Mott insulator with local moment magnetism severely limits approaches to describing some of its salient properties, such as NTE. For example, a recent work[32] presents a comparative structural diffraction and pair-distribution analysis of ScF_3 and TiF_3 data and supplements the predicted ($U=0$) band structure, which predicts a metallic state, similar to what is shown in Fig 4 for $U=J=0$. In this framework, the zone boundary Gruneisen parameters of ScF_3 are computed to be much more negative than those of TiF_3 , a difference which is ascribed to screening by the ferromagnetic half metal states, whose existence we show are inconsistent with several of our measurements. In particular, the Gruneisen parameters of both systems are calculated as a function of carrier concentration n , and a metallic state of TiF_3 is assumed to explain the weaker NTE effect in TiF_3 . The results we present in Figures 2 and 3 clearly show that $n=0$ for both systems and TiF_3 is not at all metallic. Another paper[19] interprets prior diffraction data[10] as showing NTE at low temperatures and similarly applies a $U=J=0$ density functional the-

ory calculation to describe the effect, although the original experimental authors do not in fact claim intrinsic NTE from their data. Still, in light of our conclusion of strong correlations in TiF_3 , the relative importance of zone-boundary optical phonons on the lower NTE effect in TiF_3 relative to ScF_3 must be redressed and likely would need to involve correlated electron physics.

In light of the sizable NTE in ScF_3 at all temperatures $T < 1000\text{K}$ [4] and its persistence above T_s in $\text{Sc}_{1-x}\text{Ti}_x\text{F}_3$ [25], it is of interest to consider the nature of the structural phase boundary in Figure 1a. On one end, the conventional band insulator ScF_3 harbors an incipient structural transition and displays very large and persistent NTE. On the other end, an electronically correlated insulator TiF_3 has weaker NTE above 420 K (down to -5ppm/K in one report), and strong positive thermal expansion (up to $\sim +350\text{ppm/K}$) below its structural phase transition temperature $T_s \sim 340$ K with signatures of magnetic order below 10 K. We consider here separately two possible contributors for the structural transition boundary and energy lowering of the distorted structure: (1) a cooperative Jahn-Teller effect and (2) anion dipole-dipole interactions.

In molecular octahedral coordination complexes and crystal systems based on Ti^{+3} , a significant Jahn-Teller distortion can be present[51]. Briefly, a cubic field splits the free d states into a high energy e_g orbital doublet and a lower energy t_{2g} orbital triplet manifold by a high energy scale $10D_q$. Introduction of one electron into the lower t_{2g} manifold naively produces a threefold orbital degeneracy per site, setting the circumstances for a Jahn-Teller effect, where any nonzero electron-ion interaction in principle permits a symmetry-lowering relaxation of nuclear coordinates accompanied by an orbital polarization on each site, consistent with the Jahn-Teller theorem. For TiF_3 , both prior work[39] and the electronic energy levels in Figure 4 show that a level splitting of this manifold stabilizes a single a_g state polarized along the cubic 111 direction. While the first-order, pseudo-, and second-order Jahn-Teller effects are widely considered to be present in Ti^{+3} crystals[52], their ubiquity in describing structural phase boundaries varies - having been described as negligible and irrelevant for determining ground state properties in some rare-earth titanates[53] or requiring additional considerations[54]. In the oxide perovskite LaTiO_3 for example, neutron refinement of the magnetic structure[55] and advanced theoretical considerations[56] suggest orbital fluctuations are strong, but are much weaker in YTiO_3 , suggesting a variety of importance of the Jahn-Teller effect among titanium perovskites[51]. In the present case, it is interesting to note that the phase boundary in Figure 1a terminates almost exactly at the composition which corresponds to zero d filling, as one may expect for a d -electron driven mechanism like the Jahn-Teller distortion.

On the other hand, while correlated d electron effects can certainly act in the direction of inducing a rhombohedral ground state, there is another possibility sug-

gested by a body of work addressing the $Pm\bar{3}m$ to $R\bar{3}c$ structural transition in AlF_3 at an elevated temperature of $T_s=740$ K. Because the occupied states in this system consist only of extended s - and p -derived electronic orbitals, no electron correlation effects are expected or observed, consistent with the observed diamagnetic susceptibility. This transition has been extensively studied theoretically using density functional theory[57], molecular dynamics (MD) simulations[58], and an analytical theory of anion polarizability[59] which generalizes the Clausius-Mossotti relation[60]. With the circumstances of a Jahn-Teller distortion completely absent, the driving influences of the transition in AlF_3 have been described quantitatively in terms of the long-range electric dipole-dipole interaction of the F^- anion sublattice in the distorted structure. In response to an octahedral tilt pattern relating the cubic and rhombohedral structures, direct anion displacement of the F nuclei give a *direct* nuclear dipole moment μ_D which is partially compensated by an *induced* electronic polarization μ_I for the F^- ion. The collective octahedral tilting pattern lowers the energy of the distorted structure significantly and delivers a $R\bar{3}c$ structure in the ground state. In this scenario, electrostatic Madelung energy is the dominant driver of the structural transition.

Without appealing to a Jahn-Teller mechanism, we may apply the results of the electrostatic theory to TiF_3 , since ref [59] describes an analytical theory in terms of a lattice parameter a . A surprising result for AlF_3 ($a=3.43\text{\AA}$) is that $\mu_I\sim-0.80\mu_D$, or in other words, the electronically polarized F^- induced dipole moment opposes the direct one, with about 80% cancellation of the direct displaced electric dipole. The effect of anion electronic polarizability is therefore to permit a large displacement with only a small change in the overall dipole-dipole electrostatic energy, essentially softening the associated relevant zone-boundary phonon modes considerably. Applying this analytic theory to the present case of TiF_3 , where $a = 3.88\text{\AA}$, one obtains $\mu_I\sim-0.49\mu_D$, suggesting such effects are important in this system as well. While a comparison of transition temperatures between AlF_3 and TiF_3 is limited in the framework of this theory, the curvature of the expanded potential about the cubic structure of TiF_3 is about 62% of that in AlF_3 . The observed ratio of transition temperatures is $340\text{ K}/740\text{ K}\simeq 46\%$, which would suggest a curvature ratio $\sqrt{0.46}\simeq 0.68$. While this analysis is limited, the anion dipole-dipole effects appear to account for most of

the changes in the energy landscape in comparing uncorrelated AlF_3 and correlated TiF_3 , without the need to invoke a Jahn-Teller mechanism at all.

Not mentioned in the electrostatic theory, but possibly relevant, is the potential effect of increased dielectric susceptibility due to the presence of interband transitions from d -derived bands, which may screen in part the dipole-dipole interactions and reduce the influence of the electrostatic contribution to energy lowering. Extensions of these ideas to transition metal trifluorides, and perhaps a broader class of correlated oxides, would be of value to understanding cooperative effects of Jahn-Teller and dipolar interactions in determining octahedral tilt instabilities in the important class of perovskite-based quantum materials.

In summary, the data presented here show clearly (1) that TiF_3 is an insulator, (2) that TiF_3 shows local moment spin- $\frac{1}{2}$ magnetism, (3) that TiF_3 shows magnetic features below 10 K and (4) that at least a moderate correlation parameter is required to describe the electronic structure of this system. We have suggested that Jahn-Teller effects do not act alone in driving the structural transition and anion polarizability likely plays a significant role in the physics of transition metal trifluorides. Importantly, in these open perovskites NTE materials, electron-correlated effects are present, enhancing the interest and potential applications of NTE, or materials which provide multiple functionalities and controlled thermal expansion.

ACKNOWLEDGMENTS

We acknowledge helpful discussions with Igor Maznichenko, Arthur Ernst, Pavel A. Volkov, and Angus Wilkinson. We are especially grateful to acknowledge support from the U.S. National Science Foundation, award No. NSF-DMR-1905862. R.M.G. acknowledges support from the Swedish Research Council (VR starting Grant No. 2022-03350) and Chalmers University of Technology. We also acknowledge the computing resources provided by the Center for Functional Nanomaterials, which is a U.S. DOE Office of Science Facility, at Brookhaven National Laboratory under Contract No. DE-SC0012704 and the Swedish National Infrastructure for Computing (SNIC) via the National Supercomputer Centre (NSC).

-
- [1] A. P. Ramirez, Colossal magnetoresistance, *Journal of Physics: Condensed Matter* **9**, 8171 (1997).
 [2] D. Song, M. Jeong, J. Kim, B. Kim, J. H. Kim, J. H. Kim, K. Lee, Y. Kim, and K. Char, High- k perovskite gate oxide for modulation beyond 10^{14}cm^{-2} , *Science Advances* **8**, eabm3962 (2022).
 [3] E. E. Rodriguez, A. Llobet, T. Proffen, B. C. Melot,

- R. Seshadri, P. B. Littlewood, and A. K. Cheetham, The role of static disorder in negative thermal expansion in ReO_3 , *Journal of Applied Physics* **105**, 10.1063/1.3120783 (2009).
 [4] B. K. Greve, K. L. Martin, P. L. Lee, P. J. Chupas, K. W. Chapman, and A. P. Wilkinson, Pronounced negative thermal expansion from a simple structure: Cubic

- ScF₃, *Journal of the American Chemical Society* **132**, 15496 (2010), pMID: 20958035.
- [5] J. G. Bednorz and K. A. Müller, Possible high T_c superconductivity in the Ba-La-Cu-O system, *Zeitschrift für Physik B Condensed Matter* **64**, 189 (1986).
- [6] Y. Sun, M. Kotiuga, D. Lim, B. Narayanan, M. Cherukara, Z. Zhang, Y. Dong, R. Kou, C.-J. Sun, Q. Lu, I. Waluyo, A. Hunt, H. Tanaka, A. N. Hattori, S. Gamage, Y. Abate, V. G. Pol, H. Zhou, S. K. R. S. Sankaranarayanan, B. Yildiz, K. M. Rabe, and S. Ramanathan, Strongly correlated perovskite lithium ion shuttles, *Proceedings of the National Academy of Sciences* **115**, 9672 (2018).
- [7] N. Pellet, P. Gao, G. Gregori, T.-Y. Yang, M. K. Nazeeruddin, J. Maier, and M. Grätzel, Mixed-organic-cation perovskite photovoltaics for enhanced solar-light harvesting, *Angewandte Chemie International Edition* **53**, 3151 (2014).
- [8] A. Mogoš-Milanković, J. Ravez, J.-P. Chaminade, and P. Hagenmüller, Ferroelastic properties of TF₃ compounds (T = Ti, V, Cr, Fe, Ga), *Materials Research Bulletin* **20**, 9 (1985).
- [9] S. Lee, S. Torii, Y. Ishikawa, M. Yonemura, T. Moyoshi, and T. Kamiyama, Weak-ferromagnetism of CoF₃ and FeF₃, *Physica B: Condensed Matter* **551**, 94 (2018), the 11th International Conference on Neutron Scattering (ICNS 2017).
- [10] B. J. Kennedy and T. Vogt, Powder X-ray diffraction study of the rhombohedral to cubic phase transition in TiF₃, *Materials Research Bulletin* **37**, 77 (2002).
- [11] B. A. Hunter, B. J. Kennedy, and T. Vogt, Magnetostriction in a simple trivalent manganese perovskite, *Physical Review B* **69**, 020410(R) (2004).
- [12] C. R. Morelock, L. C. Gallington, and A. P. Wilkinson, Solid solubility, phase transitions, thermal expansion, and compressibility in Sc_{1-x}Al_xF₃, *Journal of Solid State Chemistry* **222**, 96 (2015).
- [13] S. U. Handunkanda, E. B. Curry, V. Voronov, A. H. Said, G. G. Guzmán-Verri, R. T. Brierley, P. B. Littlewood, and J. N. Hancock, Large isotropic negative thermal expansion above a structural quantum phase transition, *Physical Review B* **92**, 134101 (2015).
- [14] J. M. Powell, J. Adcock, S. Dai, G. M. Veith, and C. A. Bridges, Role of precursor chemistry in the direct fluorination to form titanium based conversion anodes for lithium ion batteries, *RSC Advances* **5**, 88876 (2015).
- [15] J. Cumby, M. Burchell, and J. Attfield, High pressure synthesis, crystal growth and magnetic properties of TiOF, *Solid State Sciences* **80**, 35 (2018).
- [16] M. Umeda, Y. Tezuka, S. Shin, and A. Yagishita, Resonant photoemission study of ScF₃ at the Sc 2*p* and F 1*s* absorption edges: Observation of the satellite structure due to the strong hybridization effect, *Physical Review B* **53**, 1783 (1996).
- [17] D. Bocharov, P. Žguncs, S. Piskunov, A. Kuzmin, and J. Purans, Electronic structure of cubic ScF₃ from first-principles calculations, *Low Temperature Physics* **42**, 556 (2016).
- [18] L. Hu, J. Chen, L. Fan, Y. Ren, Y. Rong, Z. Pan, J. Deng, R. Yu, and X. Xing, Zero thermal expansion and ferromagnetism in cubic sc_{1-x}mx₃ (m = ga, fe) over a wide temperature range, *Journal of the American Chemical Society* **136**, 13566 (2014), pMID: 25233253, <https://doi.org/10.1021/ja5077487>.
- [19] L. Wang, P.-F. Yuan, F. Wang, Q. Sun, E.-J. Liang, Y. Jia, and Z.-X. Guo, Negative thermal expansion in TiF₃ from the first-principles prediction, *Physics Letters A* **378**, 2906 (2014).
- [20] D. Wendt, E. Bozin, J. Neufeind, K. Page, W. Ku, L. Wang, B. Fultz, A. V. Tkachenko, and I. A. Zaliznyak, Entropic elasticity and negative thermal expansion in a simple cubic crystal, *Science Advances* **5**, eaay2748 (2019).
- [21] C. W. Li, X. Tang, J. A. Muñoz, J. B. Keith, S. J. Tracy, D. L. Abernathy, and B. Fultz, Structural relationship between negative thermal expansion and quartic anharmonicity of cubic scf₃, *Phys. Rev. Lett.* **107**, 195504 (2011).
- [22] Z. Wei, L. Tan, G. Cai, A. E. Phillips, I. da Silva, M. G. Kibble, and M. T. Dove, Colossal pressure-induced softening in scandium fluoride, *Phys. Rev. Lett.* **124**, 255502 (2020).
- [23] I. A. Zaliznyak, E. Bozin, and A. V. Tkachenko, Comment on “colossal pressure-induced softening in scandium fluoride”, *Physical Review Letters* **126**, 179601 (2021).
- [24] C. R. Morelock, B. K. Greve, L. C. Gallington, K. W. Chapman, and A. P. Wilkinson, Negative thermal expansion and compressibility of Sc_{1-x}Y_xF₃ ($x \leq 0.25$), *Journal of Applied Physics* **114**, 213501 (2013).
- [25] C. R. Morelock, L. C. Gallington, and A. P. Wilkinson, Evolution of negative thermal expansion and phase transitions in Sc_{1-x}Ti_xF₃, *Chemistry of Materials* **26**, 1936 (2014).
- [26] S. U. Handunkanda, C. A. Occhialini, A. H. Said, and J. N. Hancock, Two-dimensional nanoscale correlations in the strong negative thermal expansion material ScF₃, *Physical Review B* **94**, 214102 (2016).
- [27] S. U. Handunkanda, E. B. Curry, V. Voronov, and J. N. Hancock, Infrared lattice dynamics in negative thermal expansion material in single-crystal ScF₃, *Journal of Physics: Condensed Matter* **32**, 035403 (2019).
- [28] C. A. Occhialini, G. G. Guzmán-Verri, S. U. Handunkanda, and J. N. Hancock, Negative thermal expansion near the precipice of structural stability in open perovskites, *Frontiers in Chemistry* **6**, 545 (2018).
- [29] A. Corrales-Salazar, R. T. Brierley, P. B. Littlewood, and G. G. Guzmán-Verri, Landau theory and giant room-temperature barocaloric effect in MF₃ metal trifluorides, *Physical Review Materials* **1**, 053601 (2017).
- [30] J. Purans, S. Piskunov, D. Bocharov, A. Kalinko, A. Kuzmin, S. E. Ali, and F. Rocca, Local structure of perovskites reo₃ and scf₃ with negative thermal expansion: interpretation beyond the quasiharmonic approximation, *Journal of Physics: Conference Series* **712**, 012013 (2016).
- [31] S. Piskunov, P. A. Žguncs, D. Bocharov, A. Kuzmin, J. Purans, A. Kalinko, R. A. Evarestov, S. E. Ali, and F. Rocca, Interpretation of unexpected behavior of infrared absorption spectra of ScF₃ beyond the quasiharmonic approximation, *Physical Review B* **93**, 214101 (2016).
- [32] F. Qin, X. Wang, L. Hu, N. Jia, Z. Gao, U. Aydemir, J. Chen, X. Ding, and J. Sun, Switch of thermal expansions triggered by itinerant electrons in isostructural metal trifluorides, *Inorganic Chemistry* **61**, 21004 (2022), pMID: 36520116.
- [33] T. A. Mary, J. S. O. Evans, T. Vogt, and A. W. Sleight, Negative thermal expansion from 0.3 to 1050 kelvin

- in *zrwi*sub $\bar{2}$ _i/sub $\bar{0}$ _jsub $\bar{8}$ _i/sub $\bar{1}$, *Science* **272**, 90 (1996), <https://www.science.org/doi/pdf/10.1126/science.272.5258.90>.
- [34] J. Chen, L. Hu, J. Deng, and X. Xing, Negative thermal expansion in functional materials: controllable thermal expansion by chemical modifications, *Chem. Soc. Rev.* **44**, 3522 (2015).
- [35] N. Shi, Y. Song, X. Xing, and J. Chen, Negative thermal expansion in framework structure materials, *Coordination Chemistry Reviews* **449**, 214204 (2021).
- [36] O. Prakash, A. Kumar, A. Thamizhavel, and S. Ramakrishnan, Evidence for bulk superconductivity in pure bismuth single crystals at ambient pressure, *Science* **355**, 52 (2017).
- [37] M. N. Gastiasoro, J. Ruhman, and R. M. Fernandes, Superconductivity in dilute SrTiO₃: A review, *Annals of Physics* **417**, 168107 (2020), Eliashberg theory at 60: Strong-coupling superconductivity and beyond.
- [38] C. Liu, X. Yan, D. Jin, Y. Ma, H.-W. Hsiao, Y. Lin, T. M. Bretz-Sullivan, X. Zhou, J. Pearson, B. Fisher, J. S. Jiang, W. Han, J.-M. Zuo, J. Wen, D. D. Fong, J. Sun, H. Zhou, and A. Bhattacharya, Two-dimensional superconductivity and anisotropic transport at KTaO₃ (111) interfaces, *Science* **371**, 716 (2021).
- [39] V. Perebeinos and T. Vogt, Jahn-teller transition in TiF₃ investigated using density-functional theory, *Physical Review B* **69**, 115102 (2004).
- [40] N. W. Ashcroft and N. D. Mermin, *Solid State Physics* (Holt-Saunders, 1976).
- [41] F. Wooten, *Optical properties of solids* (Academic Press, New York and London, 1972).
- [42] P. Hohenberg, W. Kohn, P. Hohenberg, and W. Kohn, Inhomogeneous electron gas, *Physical Review* **136**, B864 (1964).
- [43] W. Kohn and L. J. Sham, Self-consistent equations including exchange and correlation effects, *Physical Review* **140**, A1133 (1965).
- [44] G. Kresse and D. Joubert, From ultrasoft pseudopotentials to the projector augmented-wave method, *Physical Review B* **59**, 1758 (1999).
- [45] J. P. Perdew, K. Burke, and M. Ernzerhof, Generalized gradient approximation made simple, *Physical Review Letters* **77**, 3865 (1996).
- [46] H. J. Monkhorst and J. D. Pack, Special points for brillouin-zone integrations, *Physical Review B* **13**, 5188 (1976).
- [47] Y. Yekta, H. Hadipour, E. Şaşıoğlu, C. Friedrich, S. A. Jafari, S. Blügel, and I. Mertig, Strength of effective coulomb interaction in two-dimensional transition-metal halides mX_2 and mX_3 ($m = \text{Ti, V, Cr, Mn, Fe, Co, Ni}$; $x = \text{Cl, Br, I}$), *Phys. Rev. Mater.* **5**, 034001 (2021).
- [48] D. L. Esteras and J. J. Baldoví, Hubbard U library and high throughput exploration of spin Hamiltonian parameters for the rational design of metal trihalides MX₃ ($M = \{\text{Ti, V, Cr, Fe}\}$, $X = \{\text{Cl, Br, I}\}$) with high Curie temperature, arXiv:2104.03023 (2021).
- [49] J. He, S. Ma, P. Lyu, and P. Nachtigall, Unusual Dirac half-metallicity with intrinsic ferromagnetism in vanadium trihalide monolayers, *Journal of Materials Chemistry C* **4**, 2518 (2016).
- [50] S. Sachdev, *Quantum phase transitions*, second ed. ed. (Cambridge University Press, Cambridge, 2011).
- [51] K. I. Kugel' and D. I. Khomskii, The jahn-teller effect and magnetism: transition metal compounds, *Soviet Physics Uspekhi* **25**, 231 (1982).
- [52] H. Köppel, D. R. Yarkony, and H. Barentzen, *The Jahn-Teller Effect: Fundamentals and Implications for Physics and Chemistry*, Vol. 97 (Springer Science & Business Media, 2009).
- [53] J. Varignon, M. N. Grisolia, D. Preziosi, P. Ghosez, and M. Bibes, Origin of the orbital and spin ordering in rare-earth titanates, *Physical Review B* **96**, 235106 (2017).
- [54] G. Khalsa and N. A. Benedek, Ultrafast optically induced ferromagnetic/anti-ferromagnetic phase transition in gdtio3 from first principles, *npj Quantum Materials* **3**, 15 (2018).
- [55] B. Keimer, D. Casa, A. Ivanov, J. W. Lynn, M. v. Zimmermann, J. P. Hill, D. Gibbs, Y. Taguchi, and Y. Tokura, Spin dynamics and orbital state in latio₃, *Phys. Rev. Lett.* **85**, 3946 (2000).
- [56] G. Khaliullin and S. Maekawa, Orbital liquid in three-dimensional mott insulator: latio₃, *Phys. Rev. Lett.* **85**, 3950 (2000).
- [57] Y.-R. Chen, V. Perebeinos, and P. B. Allen, Density-functional study of the cubic-to-rhombohedral transition in $\alpha - \text{AlF}_3$, *Physical Review B* **69**, 054109 (2004).
- [58] S. Chaudhuri, P. J. Chupas, M. Wilson, P. Madden, and C. P. Grey, Study of the nature and mechanism of the rhombohedral-to-cubic phase transition in $\alpha\text{-AlF}_3$ with molecular dynamics simulations, *The Journal of Physical Chemistry B* **108**, 3437 (2004).
- [59] P. B. Allen, Y.-R. Chen, S. Chaudhuri, and C. P. Grey, Octahedral tilt instability of reo₃-type crystals, *Physical Review B* **73**, 172102 (2006).
- [60] P. B. Allen, Dipole interactions and electrical polarity in nanosystems: The Clausius–Mossotti and related models, *The Journal of Chemical Physics* **120**, 2951 (2004).
- [61] L. Savary and L. Balents, Quantum spin liquids: a review, *Reports on Progress in Physics* **80**, 016502 (2016).
- [62] A. P. Ramirez, Strongly geometrically frustrated magnets, *Annual Review of Materials Science* **24**, 453 (1994).
- [63] H. Sowa and H. Ahsbahs, Pressure-Induced Octahedron Strain in VF₃-Type Compounds, *Acta Crystallographica Section B* **54**, 578 (1998).
- [64] S. Mattsson and B. Paulus, Density functional theory calculations of structural, electronic, and magnetic properties of the 3d metal trifluorides MF₃ ($M = \text{Ti-Ni}$) in the solid state, *Journal of Computational Chemistry* **40**, 1190 (2019).
- [65] R. Ameis, S. Kremer, and D. Reinen, Jahn-teller effect of titanium(3+) in octahedral coordination: a spectroscopic study of hexachlorotitanate TiCl₆³⁻ complexes, *Inorganic Chemistry* **24**, 2751 (1985).
- [66] S. Maekawa, T. Tohyama, S. Barnes, S. Ishihara, W. Koshibae, and G. Khaliullin, *Physics of Transition Metal Oxides*, Springer Series in Solid-State Sciences (Springer Berlin Heidelberg, 2004).
- [67] A. V. Tkachenko and I. A. Zaliznyak, Empty perovskites as coulomb floppy networks: Entropic elasticity and negative thermal expansion, *Physical Review B* **103**, 134106 (2021).
- [68] K. Takenaka, Negative thermal expansion materials: technological key for control of thermal expansion, *Science and Technology of Advanced Materials* **13**, 013001 (2012), <https://doi.org/10.1088/1468-6996/13/1/013001>.
- [69] C. Lind, Two decades of negative thermal expansion research: Where do we stand?, *Materials* **5**, 1125–1154 (2012).